Finite-size effects in a supercooled liquid

2003 J. Phys.: Condens. Matter 15 S849

(http://iopscience.iop.org/0953-8984/15/11/309)

INSTITUTE OF PHYSICS PUBLISHING JOURNAL OF PHYSICS: CONDENSED MATTER

J. Phys.: Condens. Matter **15** (2003) S849–S858 PII: S0953-8984(03)58059-6

Finite-size effects in a supercooled liquid

Burkhard Doliwa[1] **and Andreas Heuer**[2]

[1] Max Planck Institute for Polymer Research, 55128 Mainz, Germany
[2] Institute of Physical Chemistry, University of Münster, 48149 Münster, Germany

Received 27 September 2002
Published 10 March 2003
Online at stacks.iop.org/JPhysCM/15/S849

Abstract

We study the influence of the system size on various static and dynamic properties of a supercooled binary Lennard-Jones liquid via computer simulations. In this way, we demonstrate that the treatment of systems as small as $N = 65$ particles yields results relevant for the understanding of bulk properties. In particular, we find that a system of $N = 130$ particles behaves basically as two non-interacting systems of half the size.

(Some figures in this article are in colour only in the electronic version)

1. Introduction

The theoretical understanding of the glass transition is still far from being complete. During the last few years, though, considerable progress has been made both from the analytical and from the numerical side (see, e.g., [1]). In this paper, we will dwell on some questions that arise within the framework of the energy landscape approach [2, 3]. The beauty of this technique lies in the fact that the complicated nature of many-particle effects in structurally disordered matter can be formulated in a pictorial way by considering the topology of the high-dimensional landscape of the total potential energy (PEL) $V(x)$. (Here, $x = (\boldsymbol{x}_1, \ldots, \boldsymbol{x}_N)$ denotes the set of positions of all N particles in the system.) Of special importance at low temperatures are the local minima of the PEL. They are extremely numerous, so a statistical treatment of their properties is appropriate. From the statistics of their energies and vibrational characteristics, the whole thermodynamics can be derived at low enough temperatures and constant volume [4]. Recently, generalizations to the constant-pressure situation and non-equilibrium conditions have been implemented numerically [5]. The critical temperature T_c of mode-coupling theory [6] serves as a good indicator for the temperature range where the PEL approach is appropriate: below T_c (the so-called landscape-dominated regime), it is generally accepted that the temporal evolution of a system happens through activated jumps among PEL minima. Between T_c and $2T_c$ (the landscape-influenced regime), properties of minima are generally deemed to be relevant for the thermodynamic description, whereas they are expected to be irrelevant for dynamics there. This has been concluded from the analysis of higher-order stationary points, which start to be populated above T_c [7, 8]. In two recent publications,

however, we have provided evidence that this notion should be revised: from a detailed analysis of relaxation dynamics, we have found that the picture of activated hopping is correct even above T_c [9, 10]. In any event, above $2T_c$, the PEL description breaks down, due to the fact that the system no longer occupies the well-behaved vicinity of minima.

In our recent publications, we elucidated the implications of local PEL topology for dynamics [9–11]. As conjectured by Stillinger [3], we found that the PEL is composed of groups of correlated minima, called metabasins (MBs). Diffusional motion then turned out to consist of random jumps among MBs, where the waiting times could be related to the depths of the MBs. These conclusions were drawn from computational studies of fairly small model systems of Lennard-Jones type (see [10] for details about the systems). The motivation for using systems as small as $N = 65$ particles is twofold. Firstly, much longer timescales are accessible in the simulations, and more sophisticated PEL analyses become possible [10]. Secondly, the global PEL approach implies that the hypersurface of the potential energy becomes more complex as the system becomes larger. On the other hand, generally, relaxation processes are spatially localized. This implies that PEL complexity in large systems originates mainly from a superposition of independently relaxing subsystems. In contrast, the local relaxation dynamics itself is governed by a non-trivial kind of PEL complexity which, however, is essentially identical in all the subsystems. Since we are interested in the physics behind local relaxation, we concentrate on very small systems. We thus avoid considering many relaxing subsystems in parallel which would average out the information about a single one.

In the present paper, we shall provide evidence that the results obtained in [9, 10] for a small binary Lennard-Jones system of 65 particles (BMLJ65) are also relevant for the bulk behaviour. Systems of $N = 130$, 260 and 1000 particles will be investigated and compared to the BMLJ65. In particular, we shall demonstrate that the BMLJ130 behaves essentially like two non-interacting BMLJ65s.

We shall study static quantities in section 2 and turn to dynamic observables in section 3. Further aspects of our results are discussed in section 4.

2. Static properties

2.1. Pair-correlation function

A first test for finite-size effects is to compare the distributions of interparticle distances $g_{\alpha\beta}(r)$ for different system sizes. Here, we restrict ourselves to the pair-correlation function of the A-particles, $g_{AA}(r)$; see figure 1. Within a simulation box of width L_N, we may only calculate $g_{\alpha\beta}(r)$ for $r < L_N/2$. For larger values of r, periodic images of the simulation box must be used. We find that $g_{AA}(r)$ for the BMLJ65 is identical to that of the BMLJ1000 for $r < L_{65}/2$. At larger distances, deviations from the bulk distribution can be seen. This is plausible, since the simple duplication of the simulation box can surely not reproduce all details of the long-ranged bulk correlations. Nevertheless, the oscillations corresponding to higher-order neighbour shells in the BMLJ1000 are also present in the duplicated BMLJ65. Similarly, the BMLJ130 matches the BMLJ1000 $g_{AA}(r)$ for $r < L_{130}/2$, whereas deviations for larger r already seem to be negligibly small.

2.2. Statistics of minima

How the properties of the PEL are affected by changes in system size is an important question. The most prominent characteristics of a PEL minimum are its energy ϵ and vibrational partition

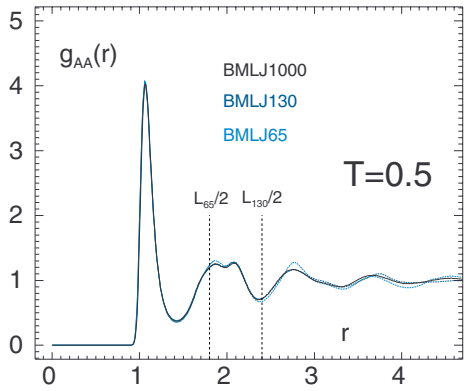

Figure 1. The pair-correlation function, $g_{AA}(r)$, for A-particles, for $N = 1000$, 130 and 65. Periodic images of the simulation box have been used to compute $g_{AA}(r)$ for distances larger than half the box width, $r > L_N/2$ ($N = 130$ and 65).

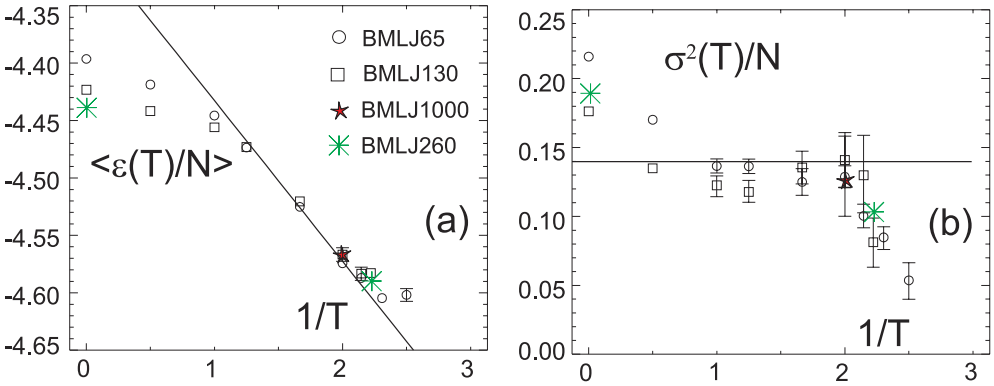

Figure 2. (a) Mean minimum energy per particle versus $1/T$. Data for different system sizes are given. (b) Variance of minimum energies, also on a per-particle basis, again versus $1/T$. The straight lines are the predictions from a Gaussian number density of minimum energies; (a) $(\epsilon_{0,\mathrm{eff}} - \beta\sigma_0^2)/N$, (b) σ_0^2/N, where $\epsilon_{0,\mathrm{eff}}$ is a constant and σ_0 the width of the distribution in equation (2). At $1/T = 0$, minimizations were performed from configurations with random particle positions.

function $T^{(3N-3)/2}Y$. The latter can be calculated within the harmonic approximation,

$$Y = \prod_{\nu} \left(\frac{2\pi}{\lambda_\nu} \right)^{1/2}, \tag{1}$$

where the λ_ν are the eigenvalues of the Hessian matrix in the minimum. Since the number of PEL minima is extremely large, a statistical treatment is needed. As a starting point, we analyse the mean energy of minima at temperature T, $\langle \epsilon(T; N) \rangle$, and their variance $\sigma^2(T; N)$. For systems composed of independent subsystems, $\langle \epsilon(T; N)/N \rangle$ and $\sigma^2(T; N)/N$ do not depend on system size. In figure 2, these quantities are shown for $N = 65$ and 130, plus some data points for $N = 260$ and 1000. As regards the mean energies, we find a good overall agreement for different system sizes. The maximum difference is about 1% between the BMLJ65 and the BMLJ260 at $T = \infty$. In the landscape-influenced regime below $T = 2T_c$, data for different N show a perfect match. A similar conclusion can be drawn from figure 2(b), where we see

$\sigma^2(T)/N$. A systematically larger value is found for the BMLJ65 at high temperatures, as compared to the BMLJ130. For $T \leqslant 2T_c$, the difference is less than 20%, but more precise statements are prohibited by the statistical uncertainty of $\sigma^2(T)/N$ below $T = 0.6$. Thus, small but significant finite-size effects can be observed in this quantity.

We briefly comment on the deviations from the Gaussian prediction at $T < 0.5$, as seen in figures 2(a), (b). The probable explanation is that our simulations below $T = 0.5$ were too short to sample the PEL thoroughly at the lowest energies. In view of the total simulation times for the BMLJ65 ($T = 0.4$: $50\tau_\alpha$; 0.435: $520\tau_\alpha$; 0.45: $850\tau_\alpha$), this is a strong statement. We currently study whether significantly longer simulations could alter the situation in figure 2, for $T < 0.5$.

2.3. Total number of minima

The overall statistics of PEL minima can be described to a large degree in terms of the number density of their energies, $G(\epsilon)$. Formally, it can be written as $G(\epsilon) = \sum_i \delta(\epsilon - \epsilon_i)$, whereas in practice, some coarse graining of energy is introduced. In computer simulations, $G(\epsilon)$ was found to be approximately Gaussian for several model systems [12–15],

$$G(\epsilon) = \frac{1}{\sqrt{2\pi\sigma_0^2}} \exp\left(\alpha N - \frac{1}{2\sigma_0^2}(\epsilon - \epsilon_0)^2\right), \qquad \epsilon > \epsilon_{\min}. \tag{2}$$

The lower cut-off energy $\epsilon_{\min}$ takes it into account that the ideal Gaussian cannot extend to arbitrarily low energies. A cut-off at the high-energetic tail of $G(\epsilon)$ is not needed, due to the small Boltzmann weight of these minima. For huge systems, which, to a good approximation, are composed of many independent subsystems, the Gaussianity of $G(\epsilon)$ is an immediate consequence of the central limit theorem. However, as discussed in [16], a large degree of Gaussianity must already be present in the subsystems that are considered elementary.

The modification of the Gaussian by the cut-off $\epsilon_{\min}$ is normally small, so one finds $N_0(N) \equiv \int \mathrm{d}\epsilon\, G(\epsilon) \approx \mathrm{e}^{\alpha N}$. Thus, the so-called growth parameter α describes how the total number of minima, $N_0(N)$, evolves with system size. We will now calculate $N_0(65)$ and $N_0(130)$. To this end, we apply a practical method which has recently been discussed in the literature [17–21]. The main step is to compute the partition function $Z(T)$ or, equivalently, the entropy via thermodynamic integration from a known reference state. The knowledge of $Z(T)$ can be used to compute $G(\epsilon)$ as follows [21]. Using the harmonic approximation of basin vibrations, the population of minimum i at temperature T is

$$p_i = \frac{1}{Z(T)} T^{(3N-3)/2} Y_i \mathrm{e}^{-\beta\epsilon_i}, \tag{3}$$

where $\beta = 1/k_B T$. By computing the expectation value $\sum_i Y_i^{-1} \mathrm{e}^{\beta\epsilon_i} \delta(\epsilon - \epsilon_i)\, p_i$, we can then extract $G(\epsilon)$:

$$\ln G(\epsilon') = \ln\langle\delta(\epsilon - \epsilon')Y^{-1}\mathrm{e}^{\beta\epsilon}\rangle + \ln Z(T) - \frac{3N-3}{2}\ln T. \tag{4}$$

In the above-cited works, starting from a high-temperature (T_0), low-density (N/V_0) state, one compressed the system until the required volume V_1 of the supercooled liquid was reached. Subsequently, one cooled along the isochore down to $T = T_1$. The procedure is depicted in figure 3(b), inset. The partition function at the state point (V_1, T_1) follows with the help of the relations

$$\begin{aligned} &\left(\frac{\partial \ln Z}{\partial V}\right)_T = \beta p(V,T), \qquad \text{and} \qquad \left(\frac{\partial \ln Z}{\partial \beta}\right)_V = -E(V,T), \\ &\ln Z(V_1,T_1) = \ln Z(V_0,T_0) + \beta_0 \int_{V_0}^{V_1} \mathrm{d}V\; p(V,T_0) - \int_{\beta_0}^{\beta_1} \mathrm{d}\beta\; E(V_1,T). \end{aligned} \tag{5}$$

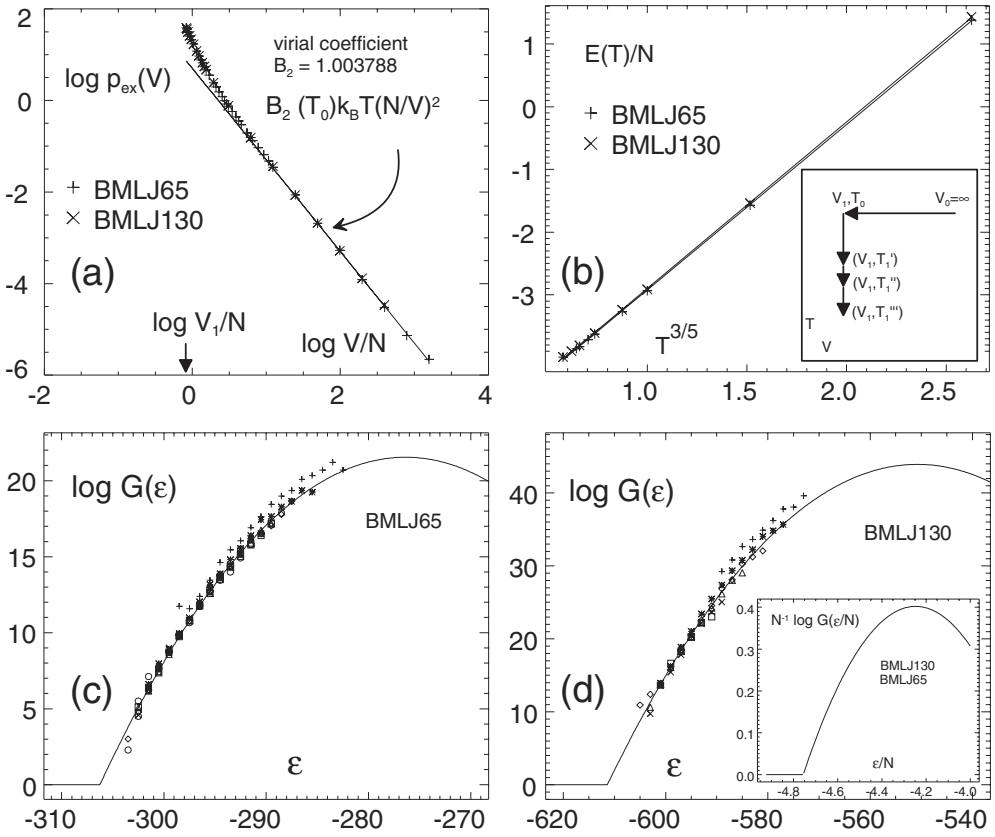

Figure 3. Determination of $G(\epsilon)$ via thermodynamic integration. (a) Excess pressure $p_{\rm ex} = p - Nk_{\rm B}T/V$ over V/N in a double-logarithmic plot. The straight line corresponds to the first correction to ideal-gas behaviour, described by the second virial coefficient $B_2(T)$. (b) The temperature dependence of the mean potential energy $E(T)/N \equiv \langle V(x)\rangle/N$. Lines are fits of the form $E(T) = a + bT^{3/5}$. Note that the data for BMLJ65 and BMLJ130 practically coincide. Inset: the thermodynamic integration path in the V–T plane ($T_0 = 5.0$, $N/V_1 = 1.2$). (c) The number density of minimum energies, $G(\epsilon)$, computed via equation (4) from simulation runs for the BMLJ65 at $T = 0.4$, 0.435, 0.45, 0.466, 0.48, 0.5 and 0.6. (d) The number density $G(\epsilon)$ of the BMLJ130, computed for $T = 0.4$, 0.435, 0.45, 0.5 and 0.6. In (c) and (d), data for $T \geqslant 0.8$ (+) do not fall on the master curve, indicating the beginning of the breakdown of the harmonic approximation. Inset: the number density of the minima of BMLJ65 and BMLJ130, on a per-particle basis. The curves coincide completely.

In the limit $V_0 \to \infty$, we may replace $\ln Z(V_0, T_0)$ in equation (5) by the ideal-gas term. Note that we write $E(V, T)$ instead of $\langle V\rangle$ for potential energy here, in order to avoid confusion with volume.

After measuring the pressure–volume dependence at $T_0 = 5$ (see figure 3(a)), we evaluate the first integral of equation (5). This yields the partition function at $T_0 = 5$, $\rho_1 = 1.2$:

$$\ln Z(V_1, T_0) = -108.3 \pm 0.7 \qquad \text{(BMLJ65)}, \tag{6}$$

$$\ln Z(V_1, T_0) = -218.5 \pm 2.5 \qquad \text{(BMLJ130)}. \tag{7}$$

Considering the second integral of equation (5), we need the mean potential energy $E(T)$ along the isochore $V = V_1$ (see figure 3(b)). As is done in the literature, we use the functional form $E(T) = a + bT^{3/5}$ to parametrize our data. For the theoretical background of this form,

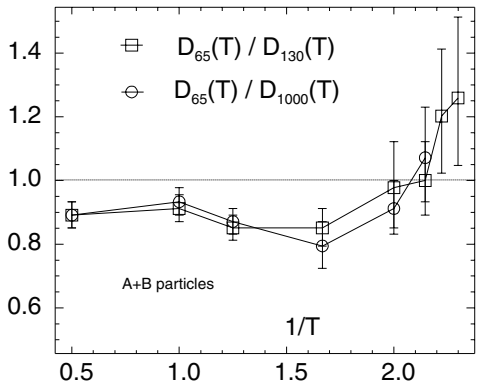

Figure 4. Ratios of diffusion coefficients $D_N(T)$ for three system sizes versus $1/T$.

see [22]. From the two fit parameters

$$a = -361.4 \pm 0.3, \qquad b = 171.5 \pm 0.3 \qquad \text{(BMLJ65)}, \tag{8}$$

$$a = -718.8 \pm 0.8, \qquad b = 341.2 \pm 0.9 \qquad \text{(BMLJ130)}, \tag{9}$$

one can then calculate the second integral in equation (5).

We now use these results to calculate N_0, via equation (4). The expectation value in equation (4) is extracted from normal simulations. Thus, as long as the harmonic approximation holds, we are able to calculate the absolute value of $G(\epsilon)$. For the BMLJ65 and BMLJ130 systems, $G(\epsilon)$ is shown in figures 3(c) and (d), respectively. At temperatures $T \leqslant 0.6$, all points for $G(\epsilon)$ fall nicely onto a master curve, whereas for $T \geqslant 0.8$ the normalization does not work any longer; see [21]. We then fit Gaussians to the data at $T \leqslant 0.6$, yielding the complete $G(\epsilon)$. The number of minima can now be calculated from $N_0 = \int \mathrm{d}\epsilon\, G(\epsilon)$:

$$N_0 = 10^{22.4 \pm 0.8} \qquad \text{(BMLJ65)}, \tag{10}$$

$$N_0 = 10^{45.0 \pm 2.5} \qquad \text{(BMLJ130)}. \tag{11}$$

Hence, within error bars, we find $N_0(130) = (N_0(65))^2$, which is the trivial scaling behaviour expected from combinations of non-interacting subsystems.

We finally note that we reached the same conclusion after calculating the configurational entropy $S_c(T; N)$ as described in [17] (data not shown here): $S_c(T; N)/N$ turns out to be identical for $N = 65$ and 130.

3. Dynamic properties

We now discuss the influence of system size on dynamics. Here, more drastic effects than in static quantities are to be expected: in fact, it is the most puzzling feature of the glass transition itself that a dramatic slowing down of molecular motion cannot be traced back to changes in static quantities easily.

3.1. Diffusion coefficients

We start with the long-time diffusion coefficient $D_N(T)$, defined by the Einstein relation. One finds that the $D_N(T)$ for $N = 65$, 130 and 1000 differ only very little. In figure 4, we see D_{65}/D_{1000} and D_{65}/D_{130} as functions of temperature. The difference between D_{65}

and D_{1000}—which we assume to be identical to the bulk diffusion coefficient—is 20% or less above T_c. Since data for D_{1000} are not available below T_c, no such comparison is possible there. The fact that the BMLJ65 is systematically slower than the bulk is in qualitative agreement with results on soft spheres. In the latter systems, though, finite-size effects are *much* more pronounced [24].

As reflected by D_{65}/D_{130}, these differences are already present between $N = 65$ and 130. Below T_c, however, the BMLJ65 seems to become slightly faster than the BMLJ130. However, since error bars are large for the two low-temperature data points, it is hard to judge whether this is a systematic effect that further increases upon cooling. In any event, in the temperature range studied, the overall variation of $D_N(T)$ is by more than three orders of magnitude. Regarding the small deviation of the BMLJ65 relative to the BMLJ1000, finite-size effects in the long-time diffusion should be judged small.

3.2. Waiting-time distributions

As a more refined comparison of dynamics between different system sizes, we consider the distributions of MB lifetimes (we use MB lifetime and waiting time as synonyms for the residence time of the system inside a MB); see [9, 23]. A detailed description of MBs and their properties can be found in [10]. Here we briefly describe how MB lifetimes can be obtained from a given simulation run. On the basis of an equidistant time series of minima, we resolve the elementary transitions between minima by further minimizations, accompanied by temporal interval bisection. From the series of configurations thus obtained, we determine the time intervals of correlated back-and-forth jumps within groups of a few minima, which are identified with the MB lifetimes [10, 11]. We detect MB lifetimes ranging from one MD step to many millions of them. At some arbitrary time of a simulation run, the probability of being in a MB of length τ is $p(\tau) = \sum_i \tau_i \delta(\tau - \tau_i)/\sum_i \tau_i$, where the τ_i are the lifetimes found in the run. (Since the MB residence times span more than six orders of magnitude, our numerical computations will involve the distributions $p(\log\tau) = p(\tau)\tau \ln 10$ rather than $p(\tau)$.) The temperature dependence of $p(\tau)$ will be suppressed for notational convenience.

Guided by the idea that a BMLJ130 system is basically a duplication of two independent BMLJ65s, we may ask whether the distribution $p_{130}(\tau)$ of the larger system can be reproduced by some sort of convolution of the distributions $p_{65}(\tau)$ of the smaller ones. (For a combined system, MB lifetimes are defined as the periods where neither of the subsystems relaxes.) Indeed, after a lengthy calculation one finds for the duplicated system

$$p_{65\otimes 65}(\tau) = -\frac{\mathrm{d}}{\mathrm{d}\tau}\int_\tau^\infty \mathrm{d}\tau'\, p_{65}(\tau') \int_\tau^\infty \mathrm{d}\tau''\, p_{65}(\tau'')\left(1 - \frac{\tau^2}{\tau'\tau''}\right). \tag{12}$$

This expression can be simplified and, upon using $p(\log\tau)$, it reads

$$p_{65\otimes 65}(\log\tau) = 2p_{65}(\log\tau)I(\tau) + 2\tau\tilde{I}(\tau)(\tilde{I}(\tau)\tau \ln 10 - p_{65}(\log\tau)), \tag{13}$$

where

$$I(\tau) = \int_\tau^\infty \mathrm{d}\tau'\, p(\tau') \qquad \text{and} \qquad \tilde{I}(\tau) = \int_\tau^\infty \mathrm{d}\tau'\, p(\tau')/\tau'.$$

In figure 5, we show $p_{65}(\log\tau)$, together with $p_{130}(\log\tau)$ at the temperature $T = 0.5$. The distribution resulting from the duplication, $p_{65\otimes 65}(\log\tau)$, is also given in the figure. It agrees reasonably well with p_{130}. Thus, on the refined level of waiting-time distributions, we find further evidence that larger systems basically behave as consisting of non-interacting BMLJ65-type building blocks. Essentially, p_{130} is shifted to the left with respect to p_{65}. This is no surprise, because time intervals where both independent systems are inert are generally shorter

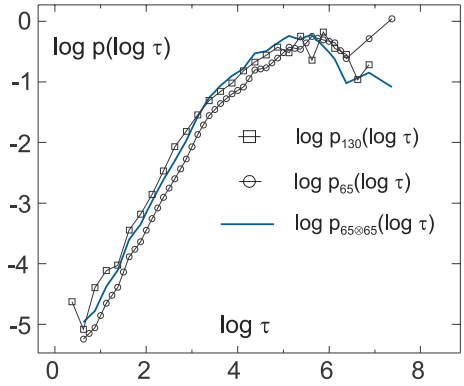

Figure 5. Distributions of MB lifetimes, $p(\log\tau)$ at $T = 0.5$. As discussed in the text, the distribution $p_{130}(\log\tau)$ should be reproducible from $p_{65}(\log\tau)$ by a special kind of convolution, equation (12). The corresponding function $p_{65\otimes65}(\log\tau)$ is given in the figure.

than the waiting times of a single system. For instance, the mean waiting times obey the relation

$$\langle\tau\rangle_{65} = 2\langle\tau\rangle_{65\otimes65},$$

which can be shown with the help of equation (12).

3.3. Metabasin depths

As discussed above, MBs have turned out to be the relevant structures in the PEL for describing the slowing down of molecular motion in supercooled liquids. In a recent paper, we reported on how the average lifetimes $\langle\tau|\epsilon_{\mathrm{MB}}; T\rangle$ of MBs depend on their energies ϵ_{MB} [10]. At some fixed ϵ_{MB}, we found that $\langle\tau|\epsilon_{\mathrm{MB}}; T\rangle$ is Arrhenius-like below $T \approx 2T_{\mathrm{c}}$, leading to the parametrization

$$\langle\tau|\epsilon_{\mathrm{MB}}; T\rangle = \tau_0(\epsilon_{\mathrm{MB}})\mathrm{e}^{\beta E_{\mathrm{app}}(\epsilon_{\mathrm{MB}})}. \tag{14}$$

The apparent activation energy $E_{\mathrm{app}}(\epsilon_{\mathrm{MB}})$ shows a strong dependence on ϵ_{MB}, as soon as one drops below $\epsilon_{\mathrm{MB}}/N \approx -4.5$. This can be seen in figure 6 where $E_{\mathrm{app}}(\epsilon_{\mathrm{MB}})$ versus ϵ_{MB}/N is depicted for both $N = 65$ and 130. Naturally, it is tempting to relate $E_{\mathrm{app}}(\epsilon_{\mathrm{MB}})$ to PEL structure. By carrying out a detailed investigation of escape paths and the barriers that are overcome when escaping the MBs, we were able to reproduce $E_{\mathrm{app}}(\epsilon_{\mathrm{MB}})$ from the local topology of MBs. Hence, we were able to prove that the effective depth $E_{\mathrm{app}}(\epsilon_{\mathrm{MB}})$ of a MB, derived from dynamics, directly corresponds to the real depth of that MB as given by the energy barriers around it. Moreover, escaping from deep MBs could be shown to involve activated jumps even above T_{c}. As regards the prefactor $\tau_0(\epsilon_{\mathrm{MB}})$ of equation (14), no such understanding in terms of PEL structure has been possible. Fortunately, however, $\tau_0(\epsilon_{\mathrm{MB}})$ turned out to have a weak dependence on MB energy. Thus, it may in good conscience be set to a constant [10].

Here we concentrate on the dependence of $E_{\mathrm{app}}(\epsilon_{\mathrm{MB}})$ on the system size. As can be seen from figure 6, the activation energies $E_{\mathrm{app}}(\epsilon_{\mathrm{MB}}/N)$ of $N = 65$ and 130 are quite close. However, the $N = 130$ data for $\epsilon_{\mathrm{MB}}/N < -4.5$ show a tendency to fall slightly below those for $N = 65$. We shall show that this trend can be understood again in terms of a simple duplication of a BMLJ65. Hence, we are interested in the combination of two independent BMLJ65 systems. Consider a MB of energy $\epsilon_{\mathrm{MB}} = \epsilon^{(1)}_{\mathrm{MB}} + \epsilon^{(2)}_{\mathrm{MB}}$ in the combined system. Then

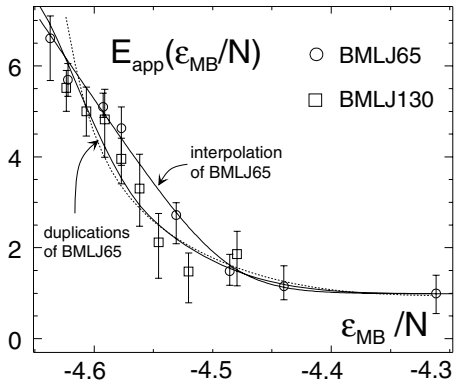

Figure 6. Apparent activation energies $E_{\rm app}(\epsilon_{\rm MB}/N)$ derived from mean lifetimes at fixed metabasin energy $\epsilon_{\rm MB}$ equation (14). Data for $N = 65$ and 130 are shown versus $\epsilon_{\rm MB}/N$. The interpolation of the $N = 65$ data has been used to compute $E_{\rm app}$ for the union of two non-interacting BMLJ65, as described in the text. The result of this calculation is given in the figure (solid curve). Three further duplications yield $E_{\rm app}$ for $N = 1040$ (dashed curve).

assume that its average lifetime can be expressed through the lifetimes of the two subsystems, i.e.

$$\frac{1}{\langle\tau|\epsilon_{\rm MB}^{(1)},\epsilon_{\rm MB}^{(2)};T\rangle_{65\otimes 65}} = \frac{1}{\langle\tau|\epsilon_{\rm MB}^{(1)};T\rangle_{65}} + \frac{1}{\langle\tau|\epsilon_{\rm MB}^{(2)};T\rangle_{65}}. \tag{15}$$

Averaging over the population of $\epsilon_{\rm MB}^{(1)}$ and $\epsilon_{\rm MB}^{(2)}$ at constant $\epsilon_{\rm MB}$ then yields $\langle\tau|\epsilon_{\rm MB};T\rangle$ for the combined system. The mean lifetimes produced in this way are again Arrhenius-like below $2T_{\rm c}$ (data not shown here). Thus, data can again be fitted by a function of the form of equation (14), yielding $E_{\rm app}(\epsilon_{\rm MB})$ for the duplicated BMLJ65. The result is shown in figure 6 for $T = 0.5$. Again, the artificial BMLJ65 duplication reproduces the observations for the real system of $N = 130$ particles.

Finally, we note that further duplication of the BMLJ65 leads to an interesting result: the activation energies from further duplications nearly fall on top of each other for $N \geqslant 130$ and $\epsilon_{\rm MB}/N > -4.6$. The example of 16 non-interacting BMLJ65s ($N = 1040$) is shown in figure 6.

4. Discussion and conclusions

For several static and dynamic observables, we have verified the factorization property

$$\text{BMLJ130} \approx \text{BMLJ65} \otimes \text{BMLJ65}.$$

The BMLJ130, in turn, seems to be close to showing bulk behaviour. Some of the results presented here have already been obtained in earlier work for a very similar Lennard-Jones-type system [12]. Again, the conclusion can be drawn that binary Lennard-Jones systems of about 60 particles are a very good compromise between the desired smallness needed for our PEL investigations and the required absence of large finite-size-related artifacts. In this connection, the simulation results of Kim and Yamamoto [24] on the standard binary soft-sphere mixture are of interest. Comparing systems of $N = 108$ and 1000 particles above $T_{\rm c}$, the authors found the small system to be up to an order of magnitude slower than the large one. These findings suggest a fundamental difference between the Lennard-Jones and soft-

sphere types of relaxation dynamics. Evidently, soft spheres exhibit a larger length scale of cooperative motion than Lennard-Jones systems. A possible explanation can be found in [12].

It is known from the study of cooperative length scales that they increase with decreasing temperature [25–27]. Thus, at some lower temperatures one might expect 65 particles to be no longer enough and finite-size effects to become visible. For a similar Lennard-Jones system it has been shown that finite-size effects are reflected by the fact that the bottom of the PEL is frequently probed [12]. In the present case still longer simulations at lower temperatures have to be performed to check whether for $N = 65$ also the PEL bottom can be reached. Then the interesting question arises of whether or not differences from the $N = 130$ system become visible.

The results presented in this paper suggest that the essential physics of the supercooled BMLJ is already contained in the system of $N = 65$ particles. For the temperatures under investigation here, extended structures of collectively moving particles ('strings') have been reported in large systems [28]. It is important to know whether these structures are still present in the small systems considered here. Work along these lines is in progress.

Acknowledgments

We are pleased to thank H W Spiess for valuable discussions. This work was supported by the DFG, Sonderforschungsbereich 262.

References

[1] Debenedetti P G and Stillinger F H 2001 *Nature* **410** 259
[2] Goldstein M 1969 *J. Chem. Phys.* **51** 3728
[3] Stillinger F H 1995 *Science* **267** 1935
[4] Stillinger F H and Weber T A 1982 *Phys. Rev.* A **25** 978
[5] Mossa S, La Nave E, Tartaglia P and Sciortino F 2002 *Preprint* cond-mat/0209181
[6] Götze W and Sjogren L 1992 *Rep. Prog. Phys.* **55** 241
[7] Angelani L, Leonardo R D, Ruocco G, Scala A and Sciortino F 2000 *Phys. Rev. Lett.* **85** 5356
[8] Broderix K, Bhattacharya K K, Cavagna A, Zippelius A and Giardina I 2000 *Phys. Rev. Lett.* **85** 5360
[9] Doliwa B and Heuer A 2002 *Preprint* cond-mat/0205283
[10] Doliwa B and Heuer A 2002 *Preprint* cond-mat/0209139
[11] Büchner S and Heuer A 2000 *Phys. Rev. Lett.* **84** 2168
[12] Büchner S and Heuer A 1999 *Phys. Rev.* E **60** 6507
[13] Sciortino F, Kob W and Tartaglia P 2000 *J. Phys.: Condens. Matter* **12** 6525
[14] Starr F W, Sastry S, La Nave E, Scala A, Stanley H E and Sciortino F 2001 *Phys. Rev.* E **6304** 041201
[15] La Nave E, Mossa S and Sciortino F 2002 *Phys. Rev. Lett.* **88** 225701
[16] Heuer A and Büchner S 2000 *J. Phys.: Condens. Matter* **12** 6535
[17] Sciortino F, Kob W and Tartaglia P 1999 *Phys. Rev. Lett.* **83** 3214
[18] Mossa S, La Nave E, Stanley H E, Donati C, Sciortino F and Tartaglia P 2002 *Phys. Rev.* E **65** 041205
[19] Sastry S 2001 *Nature* **409** 164
[20] Scala A, Starr F W, La Nave E, Sciortino F and Stanley H E 2000 *Nature* **406** 166
[21] Sastry S 2000 *J. Phys.: Condens. Matter* **12** 6515
[22] Rosenfeld Y and Tarazona P 1998 *Mol. Phys.* **95** 141
[23] Denny R A, Reichman D R and Bouchaud J-P 2002 *Preprint* cond-mat/0209020
[24] Kim K and Yamamoto R 2000 *Phys. Rev.* E **61** R44
[25] Donati C, Glotzer S C and Poole P H 1999 *Phys. Rev. Lett.* **82** 5064
[26] Bennemann C, Donati C, Baschnagel J and Glotzer S C 1999 *Nature* **399** 246
[27] Doliwa B and Heuer A 2000 *Phys. Rev.* E **61** 6898
[28] Donati C, Douglas J F, Kob W, Plimpton S J, Poole P H and Glotzer S C 1998 *Phys. Rev. Lett.* **80** 2338